Molecular Therapy
Nucleic Acids
Original Article

Improved gene therapy for MFRP deficiency-mediated retinal degeneration by knocking down endogenous bicistronic *Mfrp* and *Ctrp5* transcript

Xiao Tian,[1,5] Qingyun Zheng,[1,5] Jinyan Xie,[1] Qinlinglan Zhou,[1] Letong Liang,[1] Guotong Xu,[2] Hongyan Chen,[1] Chen Ling,[1,4] and Daru Lu[1,3]

[1]State Key Laboratory of Genetic Engineering and Engineering Research Center of Gene Technology (Ministry of Education), School of Life Sciences, Fudan University, Shanghai 200438, China; [2]Department of Ophthalmology of Tongji Hospital and Laboratory of Clinical and Visual Sciences of Tongji Eye Institute, Tongji University School of Medicine, Shanghai 200092, China; [3]NHC Key Laboratory of Birth Defects and Reproductive Health, Chongqing Key Laboratory of Birth Defects and Reproductive Health, Chongqing Population and Family Planning, Science and Technology Research Institute, Chongqing 404100, China; [4]Department of Clinical Laboratory, The First Affiliated Hospital of Wenzhou Medical University, Wenzhou, Zhejiang 325000, China

The membrane frizzled-related protein (*Mfrp*) and C1-tumor necrosis factor related protein 5 (*Ctrp5*) genes are transcribed as a bicistronic unit and dysregulation of either gene is associated with retinal degeneration in the retinal pigment epithelium (RPE) cells. However, the mechanisms that regulate the expression of the bicistronic transcript remain controversial. Here, we identified a microRNA-based negative feedback loop that helps maintain a normal expression level of the bicistronic *Mfrp* and *Ctrp5* transcript. Specifically, miR-149-3p, a conserved microRNA, binds to the 3′UTR of the *Mfrp* gene. In MFRP-deficient *rd6* mice, the miR-149-3p levels were compromised compared with those in WT mice, resulting in an increase in the bicistronic transcript. We also report a capsid-modified rAAVDJ-3M vector that is capable of robustly and specifically transducing RPE cells following subretinal delivery. Compared with the parental vector, the modified vector elicited similar levels of serum anti-rAAV antibodies, but recruited fewer microglial infiltrations. Most significantly, we also demonstrate that simultaneous overexpressing of MFRP and knockdown of the bicistronic transcript was more effective in rescuing vision than MFRP overexpression alone. Our findings offer new insights into the function of MFRP and provide a promising therapeutic strategy for the treatment of MFRP-associated ocular diseases.

INTRODUCTION

The membrane frizzled-related protein *(Mfrp)* gene encodes a type II transmembrane protein that is predominantly expressed in the retinal pigment epithelium (RPE) and ciliary body. In humans, a number of *Mfrp* mutations have now been described and linked to autosomal recessive retinitis pigmentosa (RP), a condition that is characterized by retinal spots, foveoschisis, and optic nerve head drusen.[1] Similarly, several MFRP-deficient mouse models have previously been established and shown to develop severe retinal degeneration. These mouse models include two models with spontaneous mutations in the murine orthologous *Mfrp* gene,[2,3] the retinal degeneration 6 (*rd6*) and $Mfrp^{174delG}$, and a knockin mouse model harboring a patient-derived mutant *Mfrp* gene (*Mfrp* KI/KI).[4] Among these models, *rd6* is considered an appropriate preclinical model of RP for *in vivo* treatment testing. *Rd6* mice carry a spontaneous 4-base pair (bp) deletion in the splice donor site in intron 4, which causes the skipping of exon 4 and the formation of a truncated protein. As *rd6* mice age, their photoreceptors are gradually lost, leading to a reduction in visual acuity. Histological analysis has revealed numerous aberrant cells in the subretinal space. For example, the cell layers of photoreceptors declined to four to five layers by 4.5 months, and to one layer at 24 months, while wild-type (WT) control mice retain 10–12 layers.[5] In addition, functional analysis has demonstrated a progressive reduction in the full-field electroretinogram (ERG) amplitudes in *rd6* mice.[6] Although there have been extensive studies on visual function and retinal morphology to gain detailed insights into various MFRP-deficient mouse models, the functional role of MFRP protein in RPE cells is still poorly characterized.

C1-tumor necrosis factor related protein 5 (CTRP5) is a secreted protein that plays a role in cellular adhesion and fatty acid metabolism, and mutations in this gene have been implicated in dominant late-onset

Received 25 January 2023; accepted 4 May 2023;
https://doi.org/10.1016/j.omtn.2023.05.001.

[5]These authors contributed equally

Correspondence: Hongyan Chen, State Key Laboratory of Genetic Engineering and Engineering Research Center of Gene Technology (Ministry of Education), School of Life Sciences, Fudan University, Shanghai 200438, China.
E-mail: chenhy@fudan.edu.cn
Correspondence: Chen Ling, State Key Laboratory of Genetic Engineering and Engineering Research Center of Gene Technology (Ministry of Education), School of Life Sciences, Fudan University, Shanghai 200438, China.
E-mail: lingchenchina@fudan.edu.cn
Correspondence: Daru Lu, State Key Laboratory of Genetic Engineering and Engineering Research Center of Gene Technology (Ministry of Education), School of Life Sciences, Fudan University, Shanghai 200438, China.
E-mail: drlu@fudan.edu.cn

This is an open access article under the CC BY-NC-ND license (http://creativecommons.org/licenses/by-nc-nd/4.0/).

retinal degeneration.[7] The *Mfrp* and *Ctrp5* genes are expressed as a bicistronic transcript, in which the complete open reading frame of *Ctrp5* located within the 3′-untranslated region (3′UTR) of the *Mfrp* gene.[8] It is not surprising that the MFRP and CTRP5 proteins both exist in the posterior eye, with the highest level in the RPE and ciliary body.[9] Further spatial and temporal analysis indicated subcellular co-localization and physical interaction between MFRP and CTRP5 proteins.[10,11] However, the expression pattern of the bicistronic *Mfrp* and *Ctrp5* transcript remains under investigation. It was initially reported that the bicistronic *Mfrp* and *Ctrp5* mRNA transcript was, in fact, significantly upregulated in 8-month *rd6* and $Mfrp^{174delG}$ eyecups.[3] At the protein level, while MFRP was not detectable in the $Mfrp^{174delG}$ mouse model, CTRP5 was generally upregulated at its predicted molecular weight of 26 kDa. However, microarray analysis revealed minimal change (−1.19-fold) in CTRP5 expression in the eyes of *rd6* and WT mice at ages prior to photoreceptor loss.[12] In a later study using an *Mfrp* KI/KI mouse model with a human mutant *Mfrp* gene, it was found that mRNA expression of the bicistronic *Mfrp* and *Ctrp5* genes in the posterior eyecups were 2- to 5-fold lower, compared with WT mice.[4] In another study involving patient-derived induced pluripotent stem cells (iPSC) and normal primary human RPE cells, the levels of MFRP and CTRP5 were inversely proportional to each other.[13] Most importantly, overexpression of CTRP5 in naive human RPE cells phenocopied behavior of RPE cells isolated from the MFRP-deficient patients, with both showing disorganized and elongated crisscrossing actin stress fibers, increased numbers of focal adhesions, and loss of cell-to-cell contact. In aggregate, the crosstalk between *Ctrp5* and *Mfrp* genes and the functional role of CTRP5 in the RP remain controversial.

In recent years, recombinant adeno-associated virus (rAAV)-based gene therapy has succeeded for many autosomal recessive RP diseases.[14] This fueled interest in developing additional gene therapeutics to treat numerous inherited retinal diseases, including the MFRP-deficient RP. Although many rAAV serotypes have been proven to efficiently transduce mouse photoreceptors and RPE cells,[15,16] to date, only rAAV serotype 2 (rAAV2) and serotype 8 (rAAV8) vectors were used to treat *rd6* and *Mfrp* KI/KI mice.[4,13,17–19] Previously, we designed a series of site-directed mutagenesis on rAAV capsids to enhance transduction efficiency.[20,21] Among these capsid-modified vectors, rAAVDJ-3M (N498S, Y706F, and Y732F) showed the highest efficiency in the mouse and human liver ductal organoid. Since both we[22] and others[23] recently documented that rAAVDJ vectors possessed robust transgene expression in photoreceptors and the retinal pigment epithelium, we would like to compare, side-by-side, the transduction capacity of rAAVDJ-3M vectors with that of their parental rAAVDJ vectors through subretinal and intravitreal injection.

In this study, our results showed that capsid-modified rAAVDJ-3M vectors were capable of robustly and specifically transducing RPE cells via subretinal delivery to mouse eyes. Additionally, we documented a microRNA (miRNA)-based negative feedback loop that maintains normal expression levels of the bicistronic *Mfrp* and *Ctrp5* transcript. Finally, we demonstrated the therapeutic potential of subretinal administration of an rAAVDJ-3M vector that simultaneously mediated augmentation therapy of WT MFRP and short hairpin RNA (shRNA) knockdown of the mutant bicistronic *Mfrp* and *Ctrp5* transcript. This approach rescued the retinal morphology and phenotype and preserved retinal electrophysiology in *rd6* mice. Taken together, our findings provide insights into the mechanisms underlying disease development of RP and highlight the potential of rAAV-based gene therapy for treating inherited retinal diseases.

RESULTS

Intraocular transduction characteristics and immune responses of capsid-modified rAAVDJ-3M vectors

We conducted experiments to evaluate the intraocular transduction characteristics and immune responses of capsid-modified rAAVDJ-3M vectors. Initially, we performed subretinal or intravitreal injection of rAAVDJ and rAAVDJ-3M vectors, which expressed green fluorescent protein (GFP) under a ubiquitous cytomegalovirus promoter (CMVp). At 30 days post-injection (dpi), we collected mouse eyecups and serum, and evaluated GFP expression in frozen retinal sections (Figure 1A). As expected, subretinal delivery produced more robust transgene expression in the retina than intravitreal delivery. Interestingly, the rAAVDJ-3M vectors demonstrated intense GFP signal mainly in the RPE layer, while its counterpart rAAVDJ vectors achieved strong GFP signal spanning the outer nuclear layer (ONL) and RPE. Semi-quantitative analysis of fluorescence intensity in RPE cells, shown in Figure 1B, confirmed these observations. To evaluate the immunological effects of ocular administration of different capsids, we assessed microglia infiltration in retinal frozen sections and the neutralization antibody (NAb) titers in serum. Immunofluorescence staining of ionized calcium binding adaptor molecule 1 (IBA1), a microglia activation marker, was enhanced following injection of the rAAVDJ vector, but not the AAVDJ-3M vector (Figure 1C). Meanwhile, there was no significant change in microglia population between mice that received subretinal and intravitreal injection (Figure 1D). However, we observed that rAAVDJ and rAAVDJ-3M vectors developed comparable levels of serological NAb titers at 30 dpi against rAAVDJ. Notably, subretinal administration resulted in significantly lower NAb titers for both vectors compared with intravitreal administration (Figure 1E). This is consistent with the fact that intravitreal administration is a more immunogenic route in the eye compared with subretinal administration.[24] Meanwhile, the cross-reactivity results showed that anti-rAAVDJ NAbs have lower cross-reaction with other serotypes but have higher cross-reaction with rAAVDJ-3M compared with rAAVDJ control (Figure S1).

To further evaluate the performance of the rAAVDJ-3M vector, we compared it with other rAAV capsids (rAAV2HD, rAAV8-Y733F, and rAAVDJ) that have been previously reported to promote transgene expression in retina,[23,25,26] as well as a newly modified capsid rAAV2HD-Y444F, in which the tyrosine residue was changed to phenylalanine at site 444. These vectors were delivered to mouse eyes via subretinal administration and transgene expression and microglia infiltration was determined at 30 dpi. Fluorescence analysis,

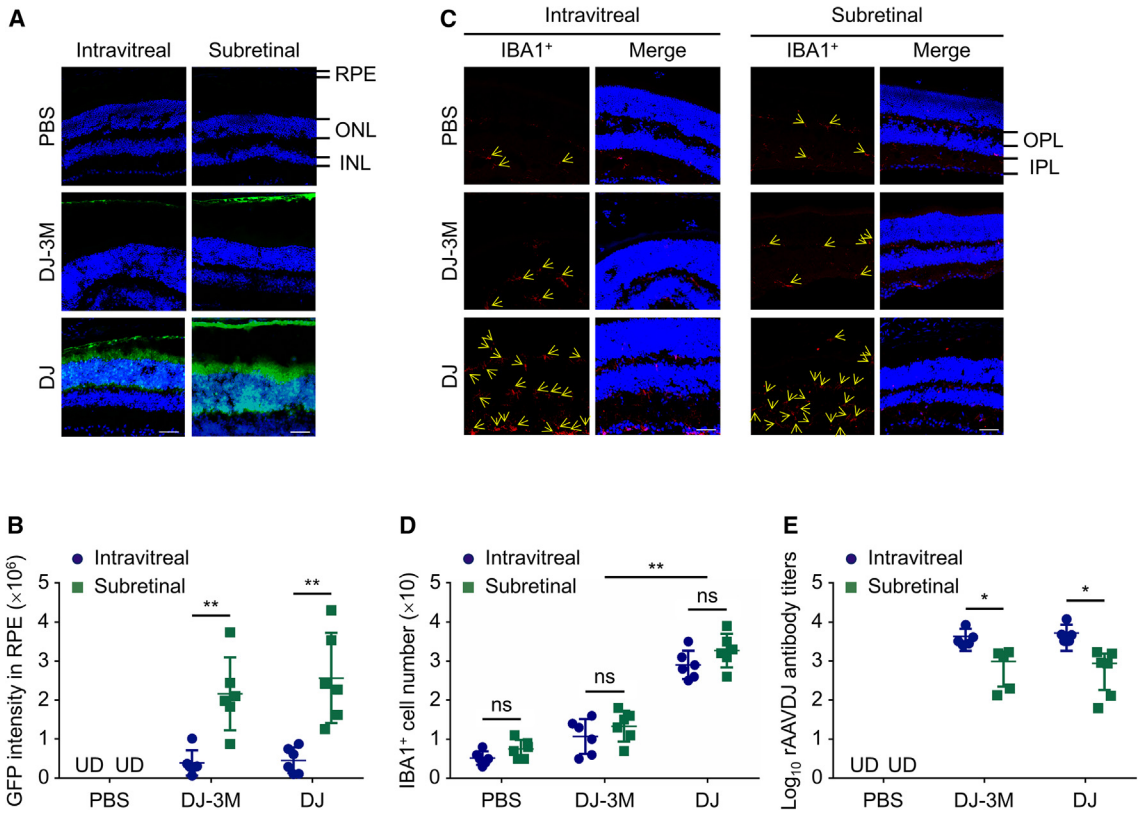

Figure 1. Analysis of transgene expression and immune responses in retinal frozen sections following subretinal or intravitreal injection with rAAVDJ and rAAVDJ-3M vectors

One microliter of rAAV-Gfp (1×10^{13} vg/mL) vector was delivered to 4-week-old WT mice by subretinal or intravitreal injection (n = 6). Mice were killed at 30 dpi, followed by collection of mouse eyecups and serum. (A) GFP fluorescence in the photoreceptors and RPE cells. Cell nuclei were stained with DAPI. (B) Quantification data of GFP expression in the RPE cells in (A). (C) Cryosections of eyes were stained with antibodies against microglia marker IBA1$^+$. Cell nuclei were stained with DAPI. Yellow arrows: IBA1$^+$ cells. (D) Quantification data of the number of IBA1$^+$ cells in the OPL and IPL in (C). (E) Neutralizing antibodies against rAAVDJ capsid in mouse serum determined by *in vitro* NAB assay. GCL, ganglion cell layer; INL, inner nuclear layer; IPL, inner plexiform layer; ONL, outer nuclear layer; OPL, outer plexiform layer; RPE, retinal pigment epithelium. Scale bar, 25 μm. **p < 0.01, *p < 0.05, *ns* means no significance.

as well as confocal scanning laser ophthalmoscopy, confirmed that subretinal delivery of the rAAVDJ and rAAVDJ-3M vectors resulted in higher GFP expression, compared with the other rAAV vectors (Figures S2, 2A, and 2B). Consistent with the above experiments, the rAAVDJ-3M vector showed GFP expression mainly in the RPE, which was superior to the commonly used rAAV8-Y733F vector. Meanwhile, the rAAVDJ vector showed widespread fluorescence signals in both the RPE and the ONL, which was further confirmed by immunostaining of rod and cone photoreceptors in retinal frozen sections (Figure S3).

In addition, immunostaining of IBA1$^+$ cells showed that all five rAAV serotypes induced more microglial cell infiltrations than PBS control (Figures 2C and 2D). It was evident that in the eyes of mice injected with rAAV2HD, rAAV8-Y733F, and rAAVDJ-3M vectors, the numbers of IBA1$^+$ cells were similar, which were much lower than those in the eyes of mice injected with rAAV2HD-Y444F and rAAVDJ vectors.

Subsequently, we extracted total genomic DNA from the RPE-choroid complexes and the vector genome copy numbers were determined by real-time quantitative PCR assays. As shown in Figure 2E, the rAAVDJ-3M vectors resulted in the highest vector genomes, followed by the rAAVDJ vector. Taken together, these results indicate that the rAAVDJ-3M vectors specifically infect the RPE layer and induces low ocular and systemic immune response, following subretinal administration.

The bicistronic *Mfrp* and *Ctrp5* transcript is significantly increased in *rd6* mice

We first compared the morphological changes in the eyes of WT and *rd6* mice. Consistent with previous reports,[5] histological analyses of 10-week-old *rd6* mouse eyes showed loss of photoreceptor cells in the ONL and shortening and disorientation of the outer segments (Figure 3A). Representative electroretinography (ERG) waveforms are shown in Figure 3B. At the studied ages, for cone-isolated b-waves, the mean amplitude of *rd6* mouse eyes was 57.5% lower

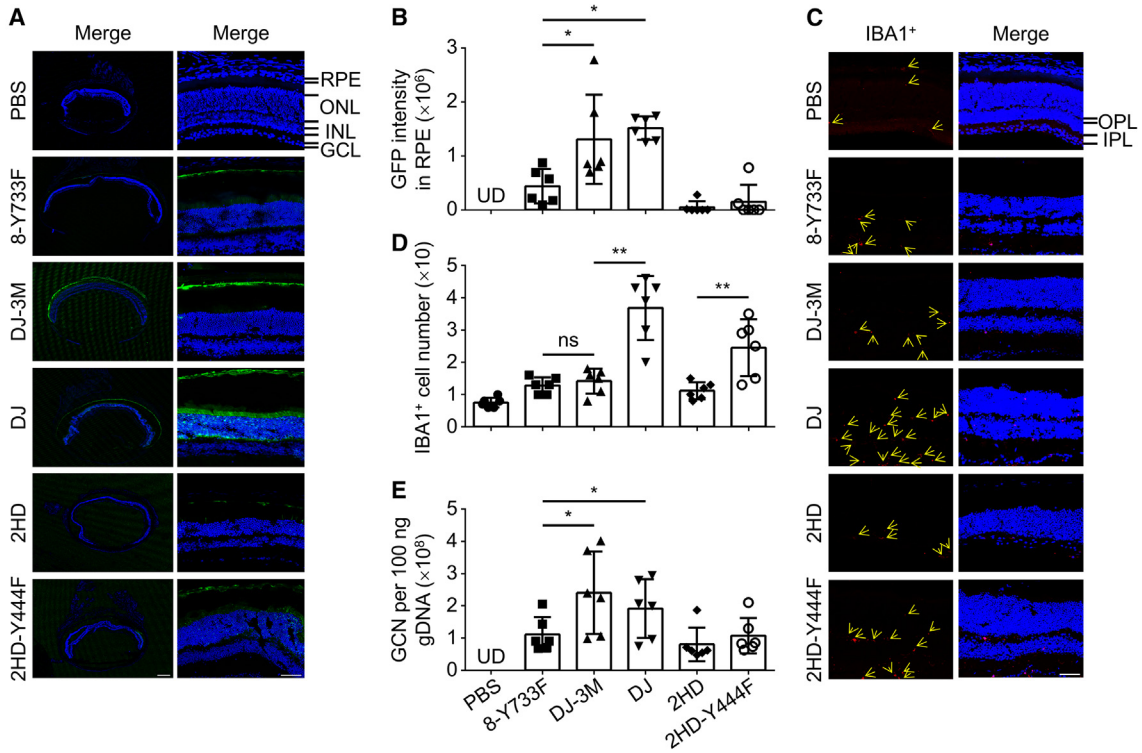

Figure 2. Comparison of rAAVDJ-3M vectors with other capsid mutants following subretinal injection

One microliter of rAAV-Gfp (1×10^{13} vg/mL) vector was delivered to 4-week-old WT mice by subretinal injection (n = 6). Mice were killed at 30 dpi, followed by collection of mouse eyecups. (A) Representative fluorescence image of ocular posterior segment (left) and retinal cross sections (right) with indicated rAAV vectors. The images were oriented with the RPE toward the top and the GCL toward the bottom. Cell nuclei were stained with DAPI. Scale bar, 250 μm (left) and 25 μm (right). (B) Quantification data of the GFP expression in the RPE cells in (A). (C) Cryosections of mouse eyes after transduction with indicated rAAV vectors were stained with antibodies against microglia marker $IBA1^+$. Cell nuclei were stained with DAPI. Scale bar, 25 μm. Yellow arrows: $IBA1^+$ cells. (D) Quantification data of the number of $IBA1^+$ cells in the OPL and IPL in (C). (E) Vector genome copy number per 100 ng gDNA was determined in the RPE-choroid complexes of rAAV-infected mouse eyes. GCL, ganglion cell layer; INL, inner nuclear layer; IPL, inner plexiform layer; ONL, outer nuclear layer; OPL, outer plexiform layer; RPE, retinal pigment epithelium. $^{**}p < 0.01$, $^{*}p < 0.05$, *ns* means no significance.

than that of WT mouse eyes, whereas *rd6* mouse eyes had abnormal amplitudes with mean values being reduced to 82.2% and 76.0% of the mean of WT for a- and b-waves of mixed rod-cone ERGs, respectively. Next, the RPE-choroid complexes of *rd6* and WT mouse eyes were collected to determine the bicistronic *Mfrp* and *Ctrp5* transcript and the CTRP5 protein levels by real-time quantitative PCR and western blot (WB) assays, respectively. To differentiate the mutant and WT *Mfrp* transcript, primer set MFRP-1 was designed to target exons 3 and 4, whereas primer set MFRP-2 was used as a control to target exons 9 and 10 (Figure 3C). As shown in Figure 3D, using primer set MFRP-1, the gene expression level of WT mouse eyes but not *rd6* mouse eyes can be detected. To our surprise, using primer set MFRP-2, the expression level of MFRP was significantly higher in *rd6* mouse eyes than that in WT mouse eyes. Similar results were observed using the primer set CTRP5. The expression levels of most other vision-related genes were not changed between WT and *rd6* mouse eyes. WB assays further corroborated the results that CTRP5 expression in the RPE-choroid complexes of *rd6* mice was significantly higher than that in the RPE-choroid complexes of WT mice, while there was no detectable CTRP5 expression in the retina (Figure 3E), consistent with previous studies showing that MFRP and CTRP5 were found to be co-localized in RPE and ciliary body.[11]

The bicistronic *Mfrp* and *Ctrp5* transcript is negatively regulated by MFRP

Next, a plasmid containing *Mfrp*-Flag was transiently transfected into two different cell lines: ARPE19 cells (a human RPE cell line) and N2A cells (a mouse neuroblast cell line). WB analysis (Figure 4A) and real-time quantitative PCR assays (Figure 4B) demonstrated that MFRP was overexpressed at both the protein and mRNA levels, respectively. This resulted in a significant reduction in the bicistronic *Mfrp* and *Ctrp5* transcript in both cell lines (Figure 4B). In contrast, truncated MFRP had little effect on *Ctrp5* expression (Figure 4C). Subsequently, we generated a rAAVDJ-3M-*Mfrp*-Flag vector, which was delivered into the eyes of 14-day-old *rd6* mouse through subretinal injection. WT mice and PBS-injected *rd6* mice were used as controls. At 60 dpi, a group of mice was killed and eyes were harvested for immunostaining assays against MFRP. Consistent with previous studies,[11] MFRP was expressed only in the RPE layer of WT mouse eyes, but not in *rd6* mouse eyes (Figure 4D).

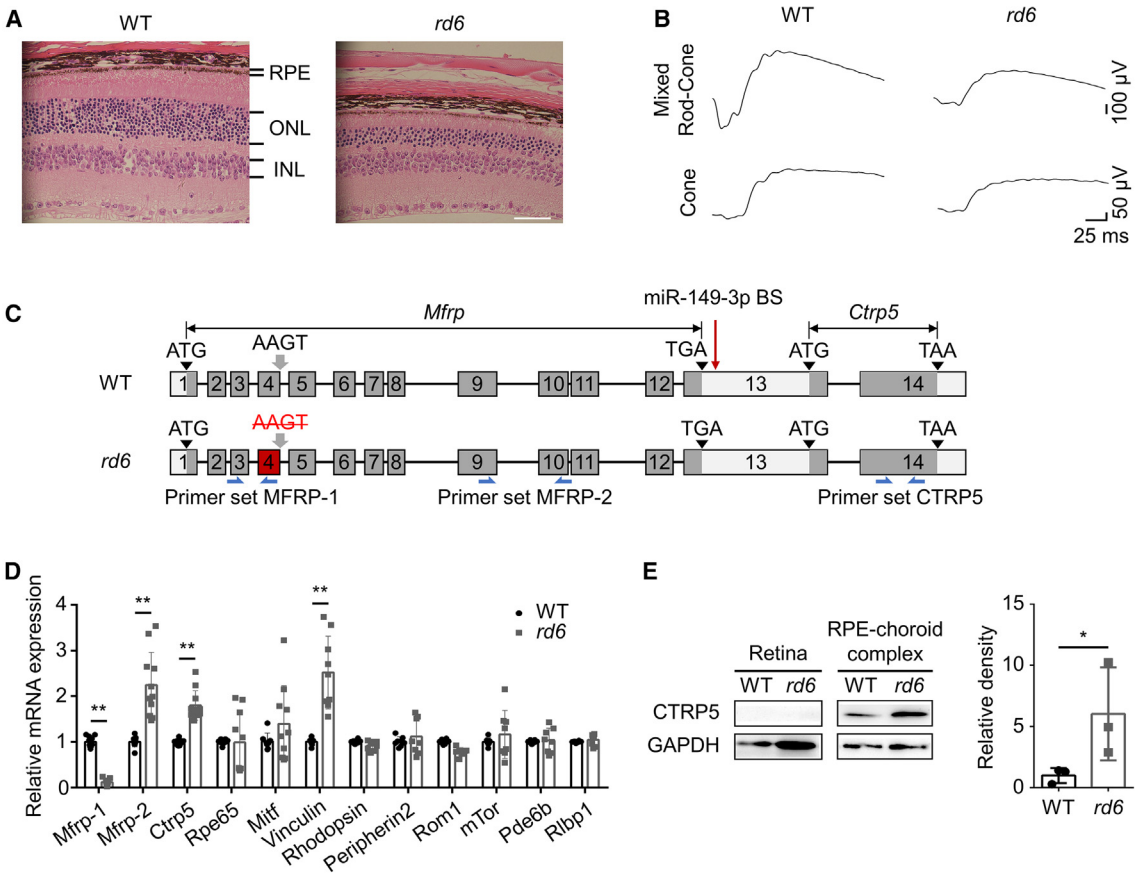

Figure 3. Structural, functional, and gene expression analysis of *rd6* mouse eyes

Ten-week-old *rd6* mice and age-matched WT mice were killed, followed by collection of mouse eyecups and RPE-choroid complexes. (A) Light microscopy of retinas in WT and *rd6* mouse eyes. (B) Representative ERG traces from WT mouse eyes compared with those from *rd6* mouse eyes. (C) Schematic representation of the bicistronic *Mfrp* and *Ctrp5* locus. The primer set MFRP-1 was used for differentiation of the WT and mutant *Mfrp* gene expression by targeting exons 3 and 4. Another primer set MFRP-2 was designed to target exons 9 and 10, which were involved in both WT and mutant *Mfrp* gene expression. The location of miR-149-3p binding site (BS, red arrow) in the 3′UTR of mouse *Mfrp* gene. (D) The mRNA expression levels of *Mfrp* and *Ctrp5*, as well as known visual system genes, from mouse eyecups and RPE-choroid complexes were profiled (n = 8). (E) The protein expression of CTRP5 in the retina and RPE-choroid complexes was determined by western blot assays (n = 3). Representative figures are shown. Meanwhile, densitometry quantification of blots was counted by ImageJ software (n = 3). INL, inner nuclear layer; ONL, outer nuclear layer; RPE, retinal pigment epithelium. Scale bar, 25 μm. $^{**}p < 0.01$, $^{*}p < 0.05$ vs. WT.

Furthermore, rAAVDJ-3M-*Mfrp*-Flag vector restored MFRP expression in the RPE layer. Another group of mice were killed, followed by collection of RPE-choroid complexes for WB assays to detect the content of CTRP5. Similar with the above *in vitro* experiments, overexpression of MFRP-FLAG *in vivo* also led to a significant reduction in CTRP5 at the protein level (Figure 4E). Taken together, our results demonstrate that MFRP inhibits the expression of bicistronic *Mfrp* and *Ctrp5* transcript.

The promoter of bicistronic *Mfrp* and *Ctrp5* genes exhibits low activity and little difference in DNA methylation pattern between WT and *rd6* mice

To explore the underlying mechanism of MFRP's inhibitory effect on the bicistronic *Mfrp* and *Ctrp5* transcript, we conducted two sets of experiments. In the first set, we cloned the −2,059-bp region upstream of the *Mfrp* gene (MFRPp) into a pGL3-Rluc/Fluc plasmid and transfected it into HEK293T and N2A cell lines along with a pGL3-CMVp-Rluc/Fluc plasmid as a control. Luciferase assay results indicated that the activity of MFRPp is approximately one-hundredth of the strong CMVp (Figure S4A). In addition, no significant reduction in luciferase expression was observed upon co-transfection of pGL3-MFRPp-Rluc/Fluc with MFRP-overexpressing plasmids into HEK293T cells (Figure S4B). In the second set of experiments, we characterized the DNA methylation pattern of the promoter of bicistronic *Mfrp* and *Ctrp5* genes. The CpG Island Searcher program (http://www.urogene.org/methprimer/) identified two potential CpG islands (from −287 bp to −546 bp) in the upstream region of the *Mfrp* gene. Total DNAs were then isolated from the RPE-choroid complexes of 10-week-old WT and *rd6* mouse eyes and the predicted CpG methylation status was confirmed by BSP, which revealed

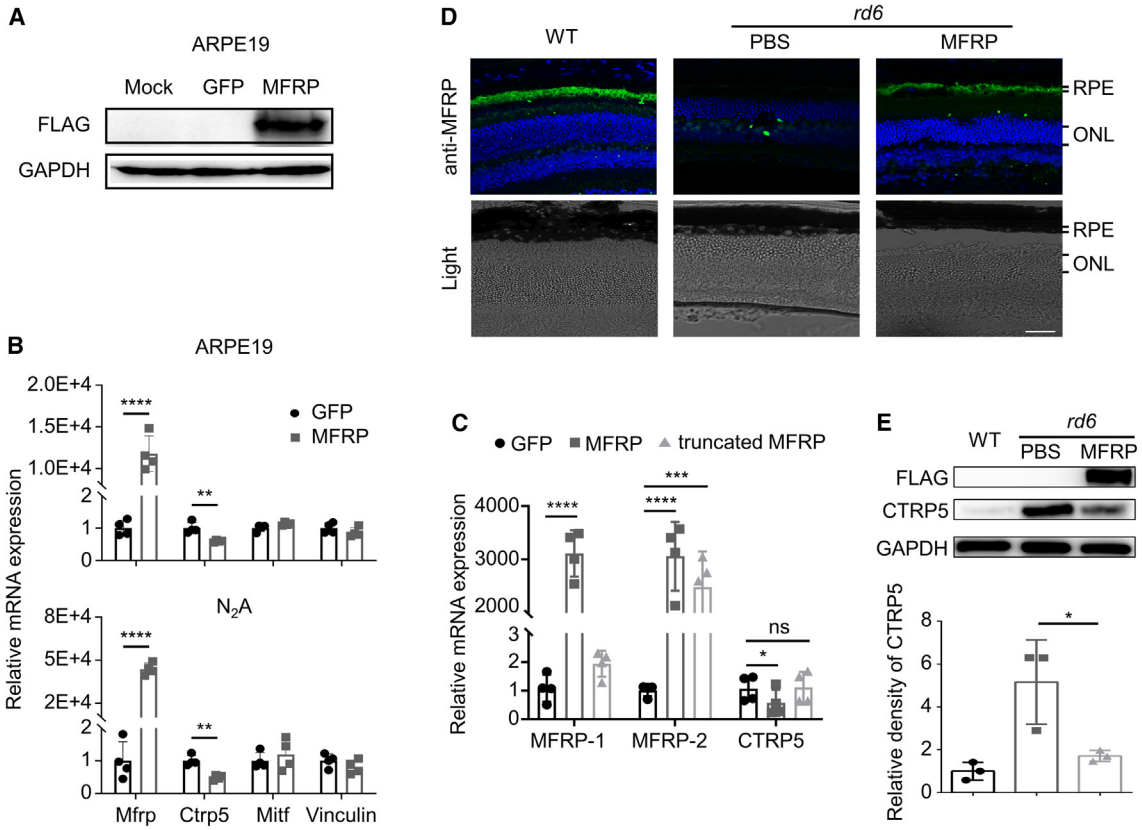

Figure 4. Overexpressing MFRP significantly reduces the bicistronic *Mfrp* and *Ctrp5* transcript

(A and B) N2A and ARPE19 cells were transfected with either MFRP-FLAG or control GFP expressing plasmid for 72 h (n = 3). (A) Protein expression levels of MFRP were determined by western blot assays using anti-FLAG antibody. (B) mRNA expression levels of *Mfrp*, *Ctrp5*, *Mitf*, and *Vinculin* were determined by real-time quantitative PCR assays (n = 4). (C) N2A cells were transfected with the plasmids containing MFRP or truncated MFRP for 72 h, with GFP plasmid as an appropriate control. The mRNA expression level of MFRP and CTRP5 was determined by real-time quantitative PCR (n = 4). (D and E) rAAVDJ-3M-*Mfrp*-Flag vector was delivered to *rd6* mouse eyes via subretinal injection (n = 3). Mice were killed at 60 dpi, followed by collection of mouse RPE-choroid complexes. MFRP and CTRP5 protein expression levels were examined by (D) immunofluorescence and (E) WB assays, respectively. Cell nuclei were stained with DAPI. Densitometry quantification of blots from (D) was measured by ImageJ software. ONL, outer nuclear layer; RPE, retinal pigmentosa epithelium. Scale bar, 25 μm. ****p < 0.0001, **p < 0.01, *p < 0.05.

similar DNA methylation levels in the MFRP promoter region of WT and *rd6* mice (Figures S4C and S4D). These results suggest that the promoter may not be involved in the MFRP's inhibitory effect on the bicistronic *Mfrp* and *Ctrp5* transcript.

MFRP inhibits the bicistronic *Mfrp* and *Ctrp5* transcript through miR-149-3p

Bioinformatics analysis was conducted to predict miRNAs that may target the bicistronic *Mfrp* and *Ctrp5* transcript. Based on three algorithms, DIANA, miRDB, and RNA22, eight potential miRNAs were identified (Figure 5A). Among them, the expression levels of miR-7081-5p and miR-149-3p were significantly reduced in the RPE-choroid complexes of *rd6* mouse eyes, compared with those of WT mouse eyes (Figure 5B). In addition, overexpressing MFRP in N2A cells significantly increased the levels of endogenous miR-7081-5p and miR-149-3p (Figure 5C). Next, we searched for the seed sequences of miR-149-3p and miR-7081-5p in different species using an online tool (Current target prediction database, miRDB: http://mirdb.org/mirdb/index.html). Our analysis revealed that mouse miR-149-3p shared the same seed sequence among eight mammalian species (Figure 5D), consistent with a recent report.[27] However, the seed sequence of miR-7081-5p in the bicistronic *Mfrp* and *Ctrp5* transcript is rodent-specific.

Indeed, when we cloned the 149BS downstream of the Fluc transgene in the pGL3-Rluc/Fluc plasmid and co-transfected it into N2A cells with miR-149-3p mimics for 48 h, a significant reduction in luciferase expression was observed upon miR-149-3p co-transfection (Figure 5E). On the other hand, when the predicted binding sites of miR-7081-5p (7081BS) were individually cloned downstream of a Fluc transgene, little change in luciferase expression was observed upon miR-7081-5p co-transfection (Figure S5). Furthermore, transfecting either miR-7081-5p or miR-149-3p mimics into N2A cells significantly reduced the levels of endogenous bicistronic *Mfrp* and *Ctrp5* transcript (Figure 5F). To investigate how MFRP regulates miR-149-3p, we performed real-time quantitative PCR assays to

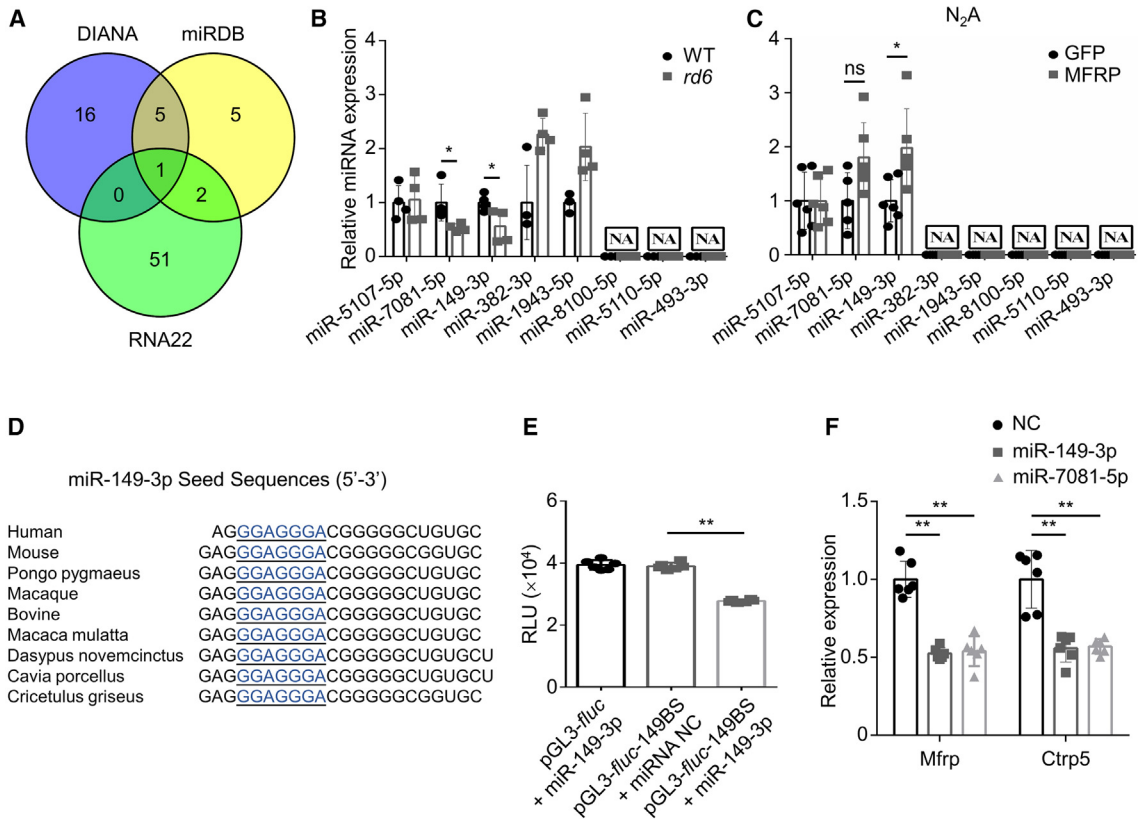

Figure 5. miR-149-3p targets the 3′UTR of the bicistronic *Mfrp* and *Ctrp5* transcript

(A) Based on three algorithms, miRDB, DIANA, and RNA22, putative miRNAs that target the bicistronic *Mfrp* and *Ctrp5* genes were identified. (B and C) Total RNA was isolated from (B) RPE-choroid complexes of 10-week-old *rd6* mice and age-matched WT mice (n = 8), or (C) N2A cells transfected with either MFRP-FLAG or control GFP expressing plasmids (n = 6). The indicated endogenous miRNA expression levels were determined by real-time quantitative PCR. (D) Sequence alignment of miR-149-3p seed region (blue bold letters) in the 3′UTR of mouse *Mfrp* gene. (E) N2A cells were transfected with the luciferase expressing plasmid containing the potential miR-149-3p binding site (BS), together with the miR-149-3p mimics. Luciferase activity assays were performed 48 h later (n = 6). (F) N2A cells were transfected with miR-7081-5p, miR-149-3p mimics, and negative control (NC) miRNA. The mRNA expression levels of endogenous *Mfrp* and *Ctrp5* genes were determined by real-time quantitative PCR using primer sets MFRP-2 and CTRP5 (n = 6). $^{**}p < 0.01$, $^{*}p < 0.05$.

examine the expression of known upstream regulators, METTL14,[28] XIST,[29] and ARAP1-AS1,[30] in the RPE-choroid complexes of WT and *rd6* mice. Our results showed undetectable endogenous XIST and ARAP1-AS1 expression. Meanwhile, the METTL14 expression in the RPE-choroid complexes of *rd6* mice was decreased compared with that of WT mice (Figure S6). Therefore, we concluded that deficiency of MFRP in *rd6* mice led to reduced miR-149-3p expression and consequently enhanced the level of bicistronic *Mfrp* and *Ctrp5* transcript.

Knocking down the bicistronic *Mfrp* and *Ctrp5* transcript *in vivo* partially rescues rod- and cone-mediated ERG function in *rd6* mice

Since overexpression of CTRP5 may have several adverse effects on human autopsy RPE, such as disorganized and elongated crisscrossing actin stress fibers, increased number of focal adhesions, and loss of cell-to-cell contact,[13] we attempted to knock down the bicistronic *Mfrp* and *Ctrp5* transcript in *rd6* mice. Four shRNAs and a non-targeting controls were synthesized, whose sequences are listed in Table S1. Each shRNA was co-transfected into HEK293T cells, together with a CTRP5-expressing plasmid. It was evident that the shRNA4 group showed the most significant reduction of CTRP5 (Figure S7). Therefore, rAAVDJ-3M-shRNA4 vector was constructed for further evaluation. It reduced the expression level of CTRP5 by 46% in the CTRP5-expressing HEK293T cells, compared with a control rAAVDJ-3M-shCon vector (Figure 6A). Next, the rAAVDJ-3M-shRNA4 vector was delivered to the eyes of 14-day-old *rd6* mice through the subretinal route. Two months after injection, a group of mice was killed and RPE-choroid complexes were collected to examine the endogenous bicistronic *Mfrp* and *Ctrp5* transcript, using the primer sets MFRP-2 and CTRP5. It was evident that the bicistronic mRNA level was significantly reduced upon rAAVDJ-3M-shRNA4 vector delivery (Figure 6B). The inhibited protein level of CTRP5 was further confirmed by WB assays (Figure 6C). To evaluate whether knocking down the bicistronic *Mfrp* and *Ctrp5* transcript could alleviate the symptom of *rd6* mice, another group of mice

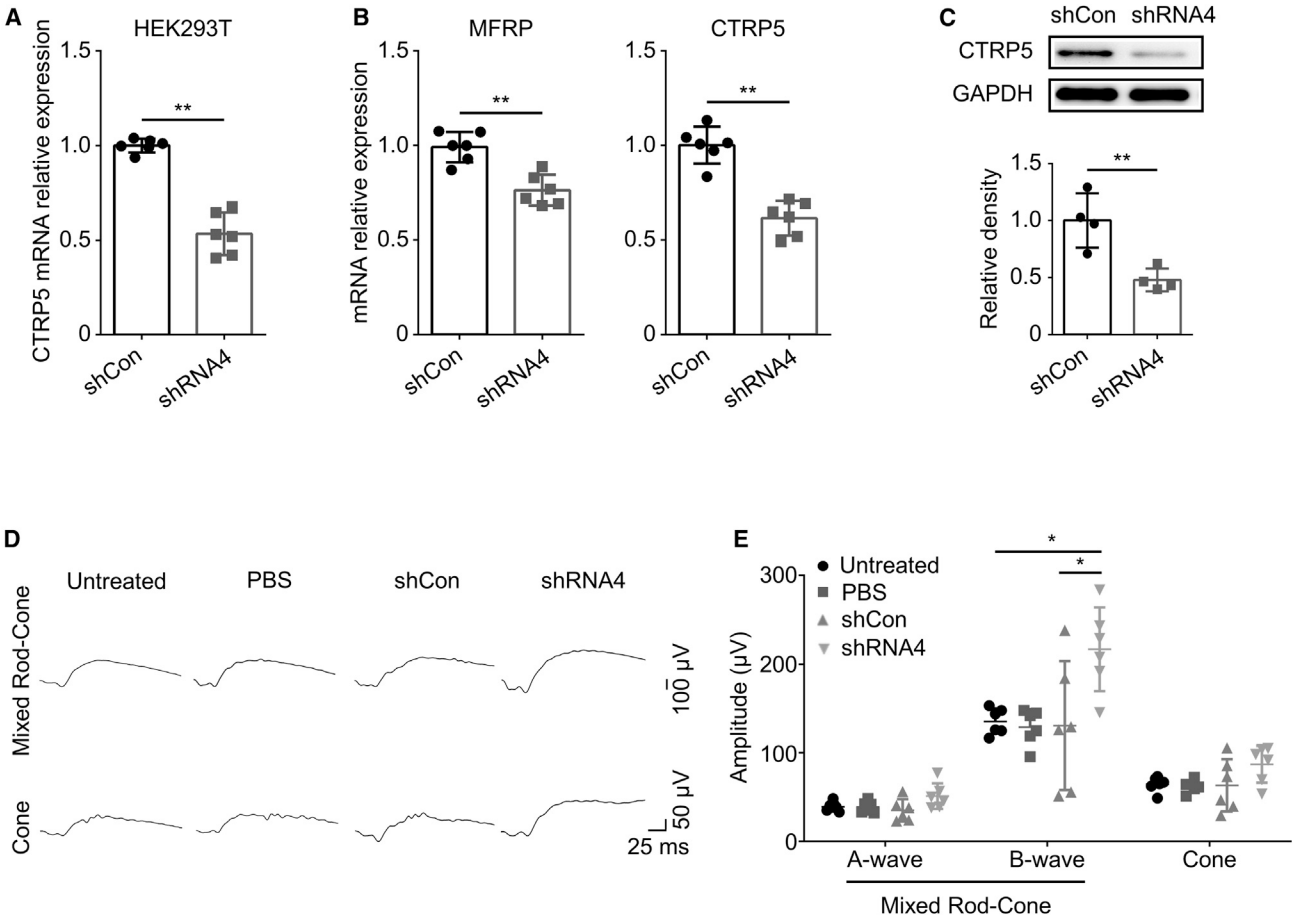

Figure 6. Knocking down the bicistronic *Mfrp* and *Ctrp5* transcript contributes to relieve the symptom of *rd6* mice

(A) HEK293T cells were transduced with rAAVDJ-3M-shRNA4 vector for 24 h, followed by transfection with CTRP5-expressing plasmid for another 48 h. The mRNA expression level of CTRP5 was determined by real-time quantitative PCR (n = 6). (B–E) One microliter of rAAVDJ-3M-shRNA4 vector or rAAVDJ-3M-shCon vector (1×10^{13} vg/mL) was delivered to 14-day-old *rd6* mouse eyes via subretinal injection. Mice were killed at 60 dpi, followed by collection of mouse RPE-choroid complexes or mouse eyecups. (B) The levels of bicistronic *Mfrp* and *Ctrp5* transcript were detected by real-time quantitative PCR using primer sets MFRP-2 and CTRP5 (n = 6). (C) The protein expression level of CTRP5 was determined by WB assays and quantified by ImageJ (n = 4). (D) Representative ERG traces from mouse eyes (n = 6). (E) Interocular difference of ERG parameters plotted for individual animals (n = 6). $^{**}p < 0.01$, $^{*}p < 0.05$ vs. shCon or untreated.

was subjected to ERG assays, with untreated *rd6* mice as the control. As shown in Figures 6D and 6E, the amplitudes of a-wave and b-wave of mixed rod-cone waveforms were increased from −35 to −51 μV and from 130 to 216 μV, respectively, and the amplitudes of cone waveforms were increased from 63 to 87 μV in rAAVDJ-3M-shRNA4 vector-injected *rd6* mouse eyes, compared with rAAVDJ-3M-shCon vector-injected *rd6* mouse eyes. In summary, our results suggest that rod- and cone-mediated ERG function can be partially rescued by reduction of the bicistronic *Mfrp* and *Ctrp5* transcript.

Simultaneously overexpressing MFRP and knocking down the bicistronic *Mfrp* and *Ctrp5* transcript effectively preserved visual function of *rd6* mice

We constructed rAAVDJ-3M-*Mfrp*-shRNA4 vectors, which contain a WT *Mfrp* cDNA and the shRNA against the bicistronic *Mfrp* and *Ctrp5* transcript. The rAAVDJ-3M-*Mfrp*-shCon vector was used as an appropriate control. Both vectors were first tested in the CTRP5-expressing HEK293T cells and resulted in a similar level of MFRP overexpression (Figure S8A). The CTRP5 level in the rAAVDJ-3M-*Mfrp*-shRNA4 vector transduced cells decreased by 57% compared with that in the rAAVDJ-3M-*Mfrp*-shCon vector transduced cells (Figure S8B).

Subsequently, both vectors and rAAVDJ-3M-*Mfrp*-Flag vector were delivered to the eyes of 14-day-old *rd6* mice via subretinal route, with untreated *rd6* mice as a control. WT mice were also used as a control. At 60 dpi, a group of mice was killed and total mRNA was isolated from the RPE-choroid complexes of mouse eyes, followed by real-time quantitative PCR to detect the expression levels of MFRP and CTRP5 (Figure 7A). Using the primer set MFRP-1 that targets the exons 3 and 4 of the *Mfrp* gene, untreated *rd6* mice showed undetectable endogenous MFRP expression. Meanwhile, both rAAVDJ-3M vectors

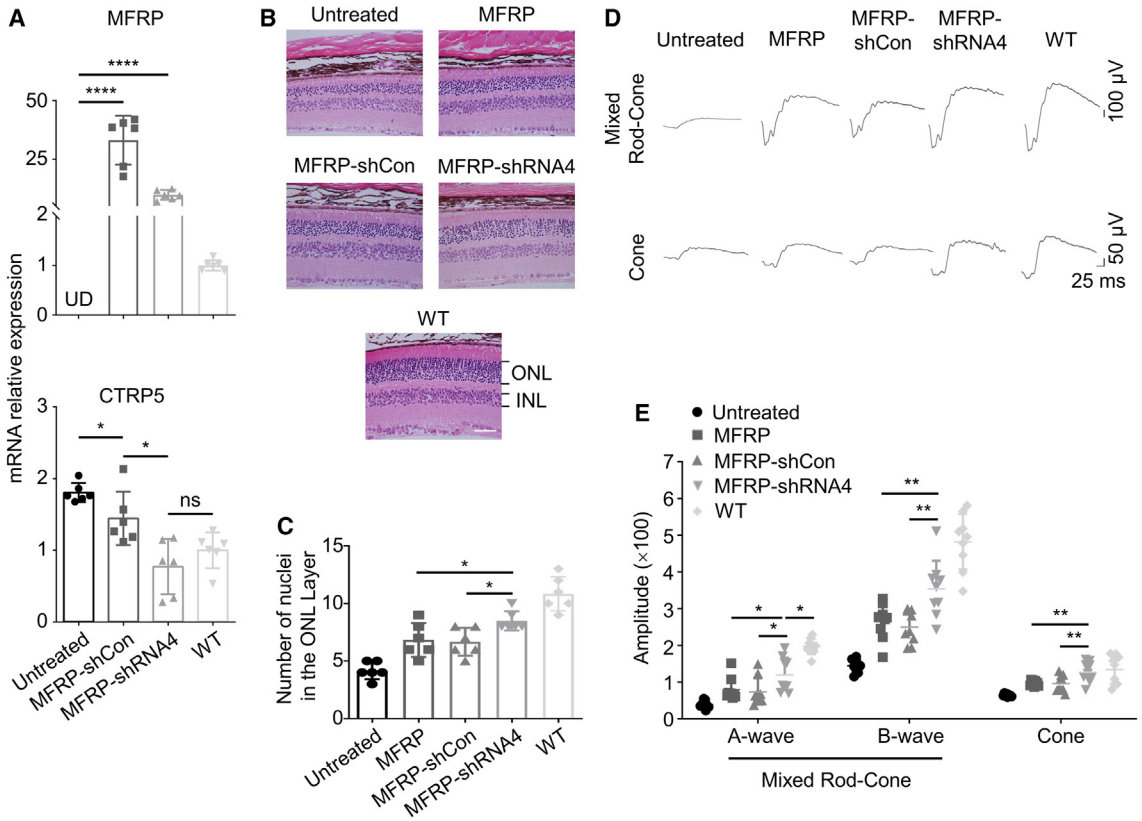

Figure 7. Combination of MFRP overexpression and bicistronic *Mfrp* and *Ctrp5* transcript knockdown provides long-term vision rescue in *rd6* mice

One microliter of rAAVDJ-3M-*Mfrp*-Flag, rAAVDJ-3M-*Mfrp*-shCon, or rAAVDJ-3M-*Mfrp*-shRNA4 vector (1×10^{13} vg/mL) was delivered to 14-day-old *rd6* mouse eyes via subretinal injection. Mice were killed at 60 dpi, followed by collection of mouse RPE-choroid complexes or mouse eyecups. (A) The levels of bicistronic *Mfrp* and *Ctrp5* transcript were detected by real-time quantitative PCR using primer sets MFRP-1 and CTRP5 (n = 6). (B) Light microscopy of retinas from different groups (n = 6) showing outer segments and ONL. (C) Mouse ONL thickness was counted (n = 6). (D) Representative ERG traces from mouse eyes (n = 9). (E) Interocular difference of ERG parameters plotted for individual animals (n = 9). ONL, outer nuclear layer. Scale bar, 25 μm. ****p < 0.0001, **p < 0.01, *p < 0.05, *ns* means no significance.

expressed exogenous MFRP at high levels. For CTRP5 expression, untreated *rd6* mice showed elevated levels compared with WT mice. Overexpression of MFRP alone by the rAAVDJ-3M-*Mfrp*-shCon vector resulted in a reduced CTRP5 level in *rd6* mouse eyes, but still higher than that in WT mouse eyes. However, simultaneous overexpression of MFRP and knockdown of the bicistronic *Mfrp* and *Ctrp5* transcript dramatically reduced CTRP5 expression to the normal level.

Another group of mice was subjected to H&E staining and ERG assays to assess retinal structure and function, respectively, with untreated *rd6* mice as a control. As shown in Figures 7B, 7C, and S8C, the butterfly diagram and statistical results showed that ONL of untreated *rd6* mouse eyes was about 4–5 nuclei thick, whereas ONL of rAAVDJ-3M-*Mfrp*-Flag-, rAAVDJ-3M-*Mfrp*-shCon-, and rAAVDJ-3M-*Mfrp*-shRNA4-injected *rd6* mouse eyes had 6–7, 6–7, and 9–10 nuclei thick, respectively. As a control, ONL of normal mouse eyes was roughly 10–12 nuclei thick. Furthermore, the amplitudes of mixed rod-cone and cone waveforms in the rAAVDJ-3M-treated *rd6* groups were significantly higher than those in the untreated *rd6* group (Figures 7D and 7E). Among all rAAVDJ-3M-treated groups, the amplitudes in mouse eyes injected with rAAVDJ-3M-*Mfrp*-shRNA4 vectors were the closest to those in WT mouse eyes. In summary, the rAAVDJ-3M-*Mfrp*-shRNA4 vector, which simultaneously overexpressed MFRP and knocked down the endogenous mutant bicistronic transcript, provided the most protective effect on retinal degeneration in *rd6* mouse eyes.

DISCUSSION

Naturally occurring rAAV capsids harboring site-directed mutations have been tested for their transduction efficiency in various retinal models, for instance, mouse[31] and canine retina,[32] human pluripotent stem cell-derived RPE cells,[33] human retinal organoids,[34] and human retinal explants.[35] Another approach to improve the native affinities of the rAAV vector is directed evolution. Both *in vitro*[36] and *in vivo*[37] directed evolutions have been conducted to improve the transduction of nonhuman primate photoreceptors dramatically. In addition, a well-known directed evolution-derived rAAV capsid, rAAVDJ, has been proved to transduce various cell types in the retina.[23] Recently, we reported that the transduction efficiency of capsids from directed evolution, such as rAAVDJ and rAAVLK03, could be further

improved by site-directed mutagenesis.[20,21] In the current study, we found that the optimized rAAVDJ-3M vector mediated detectable transgene expression primarily in the RPE layer following subretinal injection. In contrast, the parental rAAVDJ vector mediated high transgene expression spreading into the RPE, photoreceptors, and inner retinal layers. Although the triple-mutation was initially designed to increase the transduction efficiency of rAAVDJ vectors in the liver, its effects on cell tropism and retinal penetration in the eye are largely unknown. Our data suggest that the multiply mutated vectors exhibited different *in vivo* transduction properties. It is worth noticing that rAAV capsid mutants are usually thought unchangeable in terms of cell tropism compared with their WT serotypes. Therefore, our findings require further investigation in the eye. We would also like to point out that large discrepancies between laboratories have been reported despite the use of same rAAV tyrosine mutants and mouse strain.[38] It has been hypothesized that reporter genes, inconsistent vector potency from batch to batch, and other factors may contribute to inconsistent results. Thus, more repeated experiments are required to fully evaluate the rAAVDJ-3M vectors.

The rAAVDJ-3M vector not only induces less off-target effects, but also has the advantage of inducing fewer microglial infiltrations. Meanwhile it generated similar serologically neutralizing antibodies to its parental rAAVDJ vector, presumably due to the same epitope of both vectors. Microglia, the resident immune cells of the retina, are pathologically activated by many factors, such as sustained presence of tissue stress,[39] and transgene expression mediated by rAAV vectors.[40] Although the same transgene cassette was used in our side-by-side comparison, the transgene expression patterns varied between the vector capsids. This may, at least in part, explain the observed differences in microglia activation. Previous studies have shown that rAAV vectors with a photoreceptor-specific promoter may induce less microglia activation and pro-inflammatory cytokine expression,[40] although little clinical evidence of toxicity was observed using a broadly active CAG promoter.[41] Considering that MFRP is predominantly expressed in the RPE and ciliary body, the RPE-targeting rAAVDJ-3M vector together with an RPE-specific promoter would be the ideal vehicle to treat MFRP-deficient RP and warrants further investigation.

Various point mutations have been found in the human *MFRP* gene, many of which still express dysfunctional MFRP proteins[42] and subsequently increase the likelihood of endoplasmic reticulum stress. In addition, the absence of MFRP protein may lead to uncontrolled signaling by CTRP5, triggering the migration of phagocytic cells from the choroid into the subretinal space.[17] Moreover, *Ctrp5* mutations can result in an autosomal dominant negative macular degeneration, named late-onset retinal degeneration, in which significant accumulation of mutant CTRP5 was observed.[7] In a separate study, the accumulation of CTRP5 led to disorganized actin stress fibers, increased numbers of focal adhesions, and loss of cell-to-cell contact, which phenocopies the MFRP deficiency.[13] In these cases, it is necessary to knock down the endogenous bicistronic transcript with mutant genes. Currently, it is challenging to dissect the functions of *Mfrp* and *Ctrp5* genes in *rd6* mice. We observed that reducing the overexpressed CTRP5 in *rd6* mice partially prevented retinal degeneration. Considering that overexpression of CTRP5 in naive human RPE cells mimicked the pathogenesis of MFRP-deficient patient RPE cells,[13] we hypothesize that MFRP mutation and increased CTRP5 expression are both the etiological factors of ocular disease in *rd6* mice. Our studies provide a new strategy, with high recovery efficacy and low side effects because of the RPE-specific transduction of rAAVDJ-3M. In the subsequent study, the effects of prolonged treatment are worth further exploration and the retinal structure and function of different treatment groups will be evaluated after 6–12 months of treatment.

Although the association of *Mfrp* mutations with many disease phenotypes has been established, the molecular function of the MFRP protein remains unclear, partially due to the absence of any close homologs in the genome. Despite the hypothesis that MFRP and CTRP5 may function antagonistically, few mechanistic studies have been published. We found that the activity of the MFRP promoter was markedly lower than that of the strong CMV promoter, and that there were minimal differences in promoter methylation pattern between *rd6* and WT mice, lessening the likelihood of the promoter's effect on the antagonistic relationship between MFRP and CTRP5. On the other hand, our studies provide evidence that MFRP inhibits the expression of the bicistronic *Mfrp* and *Ctrp5* transcript through miR-149-3p. First, the level of miR-149-3p was significantly decreased in the RPE-choroid complexes of *rd6* mice. Second, *in vitro* overexpression of MFRP resulted in an increase of miR-149-3p content. Third, *in vitro* overexpression of miR-149-3p reduced not only the expression of endogenous bicistronic *Mfrp* and *Ctrp5* transcript, but also the luciferase expression mediated by miR-149-3p binding site that was predicted in the bicistronic transcript. Other predicted miRNAs either had undetectable levels or did not respond to MFRP overexpression. Previously, in order to obtain insight into the functional role of MFRP, gene expression profiling of WT and *rd6* mice,[12] as well as proteomic analysis among WT, *rd6,* and rAAV-*Mfrp*-treated *rd6* mice,[19] were conducted, both of which identified over 100 differentially expressed targets.

It is worth noticing that total RNAs from mouse eyes were isolated in the former study, while proteomic contents from RPE-choroid complexes were analyzed via liquid chromatography-tandem mass spectrometry in the later one. With the global prevalence of age-related eye diseases on the rise, researchers are exploring various strategies for the treatment of retinopathy.[43] Although, at this moment, the full molecular signaling pathways downstream of MFRP have not been established, these previous studies, along with our current findings, offer new insights into the function of MFRP.

MATERIALS AND METHODS

Animals

Rd6 mice (Jackson Laboratory) were provided by Professor Xu under a material transfer agreement. Age-matched C57BL/6 mice (Institute of Laboratory Animal Sciences, JSJ, China) were used as controls. All experimental mice were maintained in the animal facility of School of Life Sciences, Fudan University. Mice were

housed in a 12-h light/dark cycle, with enough water and food. The mouse procedures were approved by the Institutional Animal Care and Use Committee of Fudan University (No.: 2022JS070). All procedures were performed in accordance with the Association for Research in Vision and Ophthalmology Statement for the Use of Animals in Ophthalmic and Vision Research.

Cell lines

HEK293 (#CRL-1573), HEK293T (#CRL-3216), ARPE-19 (#CRL-2302), and N2A (#CCL-131) cells were purchased from American Type Culture Collection (Manassas, VA). Cells were cultured in Dulbecco's modified Eagle's medium (DMEM, Thermo Fisher Scientific, Waltham, USA), Dulbecco's Modified Eagle Medium/Nutrient Mixture F-12 (DMEM-F12, Thermo Fisher Scientific, Waltham, MA, USA), and opti-Minimum Essential Medium (Thermo Fisher Scientific, Waltham, MA, USA), respectively, supplemented with 10% fetal bovine serum (FBS, Thermo Fisher Scientific, Waltham, MA, USA), 100 U/mL penicillin (Thermo Fisher Scientific, Waltham, MA, USA), and 100 μg/mL streptomycin (1% P/S, Thermo Fisher Scientific, Waltham, MA, USA). Cells were maintained in an incubator at 37°C and 5% CO_2 atmosphere.

PEI-mediated plasmid transfection

The liner polyethyleneimine (PEI, Polysciences, Illinois, USA) was dissolved in deionized water as a storage solution of 1 mg/mL, and kept at −80°C. Cells were seeded into 12-well plates at a density of 80,000 cells/well and cultured for 24 h in an incubator at 37°C and 5% CO_2 atmosphere. One hour before transfection, the old medium was replaced by 500 μL/well DMEM. To make polyplex solution, 3 μL of PEI and 1 μg of plasmid DNA was individually diluted using 50 μL of DMEM. The PEI and plasmid were mixed. The polyplex solution was drop-wise added into the cell-containing plates, which were returned to the incubator at 37°C and 5% CO_2 atmosphere for 6 h. Then, the medium containing the transfection mixture was replaced by 2 mL of DMEM supplemented with 10% FBS and 1% P/S.

Plasmids

Mfrp-Flag and *Ctrp5* cDNA sequences were PCR amplified from the RPE-choroid complexes of WT mice and were subcloned into a pAAV-CMVp-Gfp plasmid driven through replacing the GFP coding sequence by *EcoRI* and *XhoI* restriction sites. The −2,059-bp region upstream of the *Mfrp* gene were PCR amplified from the RPE-choroid complexes of WT mice and was cloned into a pGL3-Rluc/Fluc plasmid through replacing the CMV promoter sequence by *SmaI* and *HindIII* restriction sites. The predicted binding sites of miR-149-3p and miR-7081-5p were synthesized and individually cloned to downstream of a Fluc transgene of pGL3-Rluc/Fluc plasmid using *BamHI* and *HindIII* restriction sites. According to the online tool (https://rnaidesigner.thermofisher.com/rnaiexpress/sort.do) and shRNA design principles, four shRNAs were designed and the interference sequences were listed in Table S1, with non-targeting sequence as control. Synthesized shRNAs were cloned to the recombinant adenoviral shuttle vector pAAV-hU6p-shCon through replacing the non-targeting sequence using *BamHI* and *HindIII* restriction sites.

Recombinant AAV vector production, purification, and titration

The rAAV capsid mutant plasmids were either reported previously[20] or constructed by a site-directed mutagenesis kit (Sangon, Shanghai, China). PEI-mediated triple-plasmid transfection method was used to produce rAAV vectors, according to a published protocol.[44] Briefly, HEK293 cells from twenty 15-cm culture plates were harvested at 72 h post transfection. The cell pellet was resuspended in 5 mL of RB TMS Buffer (50 mM Tris-HCl, 150 mM NaCl, pH 8.0), followed by three repeats of freeze in dry-ice-ethanol bath for 10 min and thaw at 37°C for 10 min, to prepare the crude lysate. The lysate was spun down at 3,000 rpm, 4°C for 10 min, and the supernatant was collected for Benzonase digestion (EMD Millipore, Darmstadt, Germany). In a 13-mL Quick-Seal centrifuge tube (Beckman Coulter, Brea, USA), the supernatant was loaded on top of iodixanol gradient (OptiPrep, Sigma-Aldrich Inc., St. Louis, USA). The samples were ultra-centrifuged at 75,000 rpm for 1 h, and the 40% iodixanol fraction was collected. The vectors were further purified by ion-exchange chromatography using HiTrap Qcolumn (GE Healthcare, Piscataway, NJ, USA), washed with phosphate-buffered saline, and concentrated using centrifugal spin concentrators with 150 K molecular weight cutoff. The vectors were finally resuspended in 500 μL PBS. The titers of Benzonase-resistant rAAV particle stocks were determined by qPCR. Briefly, 10 μL of vector stock was digested with Benzonase (EMD Millipore, Darmstadt, Germany) at 37°C for 1 h. Then, NaOH and SDS were added to make the final concentration at 100 mM and 0.2%, respectively. The samples were incubated at 65°C for 30 min. The vector DNAs were purified by DNA Clean & Concentrator-25 Kit (Zymo Research, Irvine, CA, USA) and subjected to qPCR assays to determine vector titers.

Subretinal and intravitreal injection

Subretinal injection was performed in 4-week-old WT mice or 14-day-old *rd6* mice via transvitreal approach under a surgical microscope as previously described.[22] Intravitreal injection was executed in 4-week-old WT mice. Briefly, mice were anesthetized with pentobarbitone and the ocular surface was anesthetized with proparacaine hydrochloride (0.5%). Eyes were dilated with drops of phenylephrine (0.5%) and tropicamide (0.5%). Corneal limbus at the nasal side was pierced with a 30.5-gauge BD insulin syringe needle. A 34-gauge blunt-tip needle (Hamilton, Reno, NV, USA) was introduced into subretinal space or vitreous chamber through the corneal incision. Each eye received 1 μL rAAV solution at a titer of 1×10^{13} vg/mL, or equal volume of PBS. After injection, the needle was held in place for a few seconds to allow full treatment delivery before being slowly withdrawn. Subsequently, the eye ointment was applied to the ocular surface after intraocular surgery to prevent postoperative infection. Mice were placed in a 37°C incubator for 1 h and then returned to the original position.

rAAV vector genome copy number quantification

Fresh RPE-choroid complexes were snap-frozen in dry ice-cooled isopentane and genomic DNA was extracted from tissue samples by a DNA extraction kit (Tsingke, Beijing, China). Vector genome copy number per ng of genomic DNA was determined by qPCR assays using

SYBR Green kit (Toyobo, Osaka, Japan). The absolute amount was obtained by referring to a standard curve consisting of a 10-fold serial dilution of the known amount of respective proviral *cis* plasmids. The primer set was designed for the ITR region. The forward primer is 5′- GGAACCCCTAGTGATGGAGTT-3′ and the reverse primer is 5′- CGGCCTCAGTGAGCGA-3′, which are listed in Table S1.

Neutralizing antibody assay

Serum was obtained when the animals were killed. Cells were seeded into 96-well plates at a density of 50,000 cells/well and cultured for 24 h in an incubator at 37°C and 5% CO_2 atmosphere. The rAAVDJ-Fluc vectors were diluted in serum-free DMEM and incubated with serial dilutions of the serum samples for 30 min at 37°C. Subsequently, the serum-vector mixtures were added to the cells at a multiplicity of infection of 1,000 vg/cell. After 48 h, cells were lysed using the One-Lite Luciferase Assay Kit (Vazyme, Nanjing, China) and luciferase activity was measured on a luminometer (BioTek, Winooski, USA) as relative light units per second. The neutralizing titer was reported as the highest serum dilution that inhibited rAAV transduction by $\geq$50% compared with the 100% transduction control.

RNA isolation and qPCR

Total RNA was extracted from RPE-choroid complexes using the RNA extracting kit (Takara, Osaka, Japan). cDNA was synthesized from 1 μg RNA using PrimeScript Reverse Transcriptase Master Mix (Takara, Osaka, Japan). qPCR reactions were performed using SYBR Green kit (Toyobo, Osaka, Japan), with gene-specific primer sets (Table S1). The efficiency of each pair of primers ranged from 90% to 110% based on qPCR assays (Figure S9). Relative mRNA expression was calculated using the ΔΔCT method and normalized against reference gene (GAPDH) in each sample.

Immunofluorescence

Immunofluorescence was performed for both whole mounts and transverse sections of the retina.[45] Briefly, retinal cryosections were blocked in 0.5% Triton X-100 and 5% bovine serum albumin in PBS for 1 h at room temperature. Afterward, sections were incubated overnight at 4°C with primary antibodies for anti-IBA1$^+$ (019–19741, 1:1000, Wako, Tokyo, Japan), anti-Rhodopsin (MAB5356, 1:500, Merck, Darmstadt, German), anti-Cone arrestin (AB15282, 1:1000, Merck, Darmstadt, German), and anti-MFRP (AF3445, 1:40, R&D, Minnesota, USA). After washing three times with PBST (1% Tween 20 in PBS), samples were incubated with Alexa 594 (ab150080/ab150116, 1:1000, Abcam, Cambridge, MA, USA) or FITC (PA1-28734, 1:1000, Thermo Fisher Scientific, Waltham, MA, USA) secondary antibodies for 1 h. Subsequently, sections were washed three times with PBS and stained with DAPI. Images were captured using an Olympus FV3000 confocal microscope. The number of infiltrated microglia and GFP density in the RPE layer were quantified by IMARIS software.

WB analysis

Total proteins were extracted from cells or RPE-choroid complexes by lysis buffer (Beyotime, Shanghai, China) and quantified by BCA Protein Assay Kit (Beyotime, Shanghai, China). Samples were separated using 10% SDS-PAGE electrophoresis and transferred to PVDF membrane. The membrane was blocked with 5% skimmed milk in PBST for 1 h and incubated overnight at 4°C with anti-CTRP5 (503021, 1:1000, ZEN bioscience, Chengdu, China), anti-FLAG (14793, 1:1000, Cell Signaling Technology, Boston, MA, USA) or anti-GAPDH (ab181602, 1:2000, Abcam, Cambridge, MA, USA) antibodies. After washing with PBST, the membrane was incubated with horseradish peroxidase-conjugated secondary antibodies at 1:5,000 for 1 h at room temperature. The membrane was detected with an enhanced chemiluminescence substrate and the blots were captured using automatic chemiluminescence imager (Tanon, Shanghai, China).

Electroretinography

Full-field electroretinography (ERG) was carried out to measure scotopic a- and b-wave and photopic b-wave amplitudes. All experimental operations were performed under dim red light. Briefly, mice were dark-adapted overnight and anesthetized with pentobarbitone. Pupils were dilated with phenylephrine (0.5%) and tropicamide (0.5%). Dark-adapted ERGs were elicited with 0.01 scot-cd•sec•m^{-2} and 2 scot-cd•sec•m^{-2}. In addition, cone-isolated ERGs were elicited with 2 scot-cd•sec•m^{-2} with a 25 scot-cd•sec•m^{-2} background light for 10 min. ERG measurements were made using the APS-2000AER system (Kanghua, Chongqing, China). The a-waves were measured from baseline to the trough of the downward deflecting wave, whereas the b-waves were taken from trough of the a-wave to the peak of upward deflecting wave. Analysis of variance (ANOVA) was used to determine the statistical significance between waveform amplitudes in various groups. At least 6–10 mice were detected in each group.

Histological analysis

Retinal morphology and photoreceptor structure were assessed at 60 dpi by histological analysis. In brief, eyecups were dissected, fixed in 4% paraformaldehyde, and embedded in paraffin. Paraffin sections were at 4-μm thickness and stained with H&E for structural integrity. The butterfly diagram and images were captured using a microscope (Nikon, Tokyo, Japan).

Bisulfite sequencing

DNA methylation of MFRP promoter sequence from the RPE-choroid complexes of *rd6* and WT mice was determined by bisulfite sequencing PCR. Two micrograms of purified genomic DNA was bisulfite-converted and purified using EpiTect Bisulfite Kit (Qiagen, Dusseldorf, Germany). Purified bisulfite-converted DNA was amplified by the designed primer set (Table S1) using Epi Taq (Takara, Osaka, Japan) and purified PCR products were cloned into pMD18-T vectors (Takara, Osaka, Japan). Afterward, colonies were selected and sequenced by Sanger sequencing.

Luciferase reporter assay

Cells were seeded in 96-well or 12-well plates and transfected using PEI according to the manufacturer's instructions 48 h after

transfection. Cells were lysed with 100 μL of lysis reagent (Promega, Madison, WI, USA). Firefly and Renilla luciferase expression was assessed using a luminometer (BioTek, Winooski, VT, USA) according to the Dual-Luciferase Reporter Assay System (Promega, Madison, WI, USA). Briefly, after thawing frozen samples at room temperature, 10 μL of lysates was added into a 96-well plate, followed by adding 10 μL of luciferase assay reagent (Promega, Madison, WI, USA). The plate was placed in a luminometer at room temperature. The delay and measurement times were set for 2 and 10 s, respectively. All measurements were finished within 15 min. All the luciferase reporter assays were calculated as the ratio between firefly and Renilla luciferase activities. The pGL3-Rluc/Fluc plasmid contained a Renilla luciferase under the control of T7 promoter. Data generated from three independent experiments were used for comparison.

Statistical analysis

All experimental data were presented as the mean ± standard deviation (SD). Unpaired Student's t test, Tukey's test, or ANOVA was applied to compare the difference of different groups. Tests were performed on GraphPad Prism 6 (GraphPad Software, USA). $p < 0.05$ was considered statistically significant.

DATA AVAILABILITY

All data included in this study are available upon request.

SUPPLEMENTAL INFORMATION

Supplemental information can be found online at https://doi.org/10.1016/j.omtn.2023.05.001.

ACKNOWLEDGMENTS

We would like to thank Prof. Guotong Xu for providing free *rd6* mice. This work is sponsored by grants from the National Key Research and Development Program of China (#2021YFC2301500, to C.L.), the National Natural Science Foundation of China (#81972713, to C.L.), Key Project of Chongqing Natural Science Foundation (cstc2020jcyj-zdxm0180, to D.L.). C.L. is supported by the Oriental Scholars of Shanghai Universities (GZ2020001).

AUTHOR CONTRIBUTIONS

D.L., H.C., and C.L. designed the project. X.T., Q.Z., J.X., Q.Z., and L.L. performed the experiments. X.T. and Q.Z. analyzed the data and generated figures. G.X. provided technical advice. X.T., Q.Z., Q.Z., and C.L. wrote the manuscript. All authors read and approved the final manuscript.

DECLARATION OF INTERESTS

The authors declare no competing interests.

REFERENCES

1. Ren, X., Gao, Y., Lin, Y., Fu, X., Xiao, L., Wang, X., Zeng, Z., Bao, L., Yan, N., Zhang, M., and Tang, L. (2022). A novel mutation in the membrane frizzled-related protein gene for posterior microphthalmia, non-pigmented retinitis pigmentosa, optic nerve drusen, and retinoschisis in a consanguineous family. Front. Med. *9*, 835621.
2. Kameya, S., Hawes, N.L., Chang, B., Heckenlively, J.R., Naggert, J.K., and Nishina, P.M. (2002). Mfrp, a gene encoding a frizzled related protein, is mutated in the mouse retinal degeneration 6. Hum. Mol. Genet. *11*, 1879–1886.
3. Fogerty, J., and Besharse, J.C. (2011). 174delG mutation in mouse MFRP causes photoreceptor degeneration and RPE atrophy. Invest. Ophthalmol. Vis. Sci. *52*, 7256–7266.
4. Chekuri, A., Sahu, B., Chavali, V.R.M., Voronchikhina, M., Soto-Hermida, A., Suk, J.J., Alapati, A.N., Bartsch, D.U., Ayala-Ramirez, R., Zenteno, J.C., et al. (2019). Long-term effects of gene therapy in a novel mouse model of human MFRP-associated retinopathy. Hum. Gene Ther. *30*, 632–650.
5. Hawes, N.L., Chang, B., Hageman, G.S., Nusinowitz, S., Nishina, P.M., Schneider, B.S., Smith, R.S., Roderick, T.H., Davisson, M.T., and Heckenlively, J.R. (2000). Retinal degeneration 6 (rd6), a new mouse model for human retinitis punctata albescens. Invest. Ophthalmol. Vis. Sci. *41*, 3149–3157.
6. Won, J., Smith, R.S., Peachey, N.S., Wu, J., Hicks, W.L., Naggert, J.K., and Nishina, P.M. (2008). Membrane frizzled-related protein is necessary for the normal development and maintenance of photoreceptor outer segments. Vis. Neurosci. *25*, 563–574.
7. Chekuri, A., Zientara-Rytter, K., Soto-Hermida, A., Borooah, S., Voronchikhina, M., Biswas, P., Kumar, V., Goodsell, D., Hayward, C., Shaw, P., et al. (2019). Late-onset retinal degeneration pathology due to mutations in CTRP5 is mediated through HTRA1. Aging Cell *18*, e13011.
8. Hayward, C., Shu, X., Cideciyan, A.V., Lennon, A., Barran, P., Zareparsi, S., Sawyer, L., Hendry, G., Dhillon, B., Milam, A.H., et al. (2003). Mutation in a short-chain collagen gene, CTRP5, results in extracellular deposit formation in late-onset retinal degeneration, a genetic model for age-related macular degeneration. Hum. Mol. Genet. *12*, 2657–2667.
9. Ayyagari, R., Mandal, M.N.A., Karoukis, A.J., Chen, L., McLaren, N.C., Lichter, M., Wong, D.T., Hitchcock, P.F., Caruso, R.C., Moroi, S.E., et al. (2005). Late-onset macular degeneration and long anterior lens zonules result from a CTRP5 gene mutation. Invest. Ophthalmol. Vis. Sci. *46*, 3363–3371.
10. Mandal, M.N.A., Vasireddy, V., Reddy, G.B., Wang, X., Moroi, S.E., Pattnaik, B.R., Hughes, B.A., Heckenlively, J.R., Hitchcock, P.F., Jablonski, M.M., and Ayyagari, R. (2006). CTRP5 is a membrane-associated and secretory protein in the RPE and ciliary body and the S163R mutation of CTRP5 impairs its secretion. Invest. Ophthalmol. Vis. Sci. *47*, 5505–5513.
11. Mandal, M.N.A., Vasireddy, V., Jablonski, M.M., Wang, X., Heckenlively, J.R., Hughes, B.A., Reddy, G.B., and Ayyagari, R. (2006). Spatial and temporal expression of MFRP and its interaction with CTRP5. Invest. Ophthalmol. Vis. Sci. *47*, 5514–5521.
12. Soundararajan, R., Won, J., Stearns, T.M., Charette, J.R., Hicks, W.L., Collin, G.B., Naggert, J.K., Krebs, M.P., and Nishina, P.M. (2014). Gene profiling of postnatal Mfrprd6 mutant eyes reveals differential accumulation of Prss56, visual cycle and phototransduction mRNAs. PLoS One *9*, e110299.
13. Li, Y., Wu, W.H., Hsu, C.W., Nguyen, H.V., Tsai, Y.T., Chan, L., Nagasaki, T., Maumenee, I.H., Yannuzzi, L.A., Hoang, Q.V., et al. (2014). Gene therapy in patient-specific stem cell lines and a preclinical model of retinitis pigmentosa with membrane frizzled-related protein defects. Mol. Ther. *22*, 1688–1697.
14. Maguire, A.M., Bennett, J., Aleman, E.M., Leroy, B.P., and Aleman, T.S. (2021). Clinical perspective, treating RPE65-associated retinal dystrophy. Mol. Ther. *29*, 442–463.
15. Lee, J.H., Wang, J.H., Chen, J., Li, F., Edwards, T.L., Hewitt, A.W., and Liu, G.S. (2019). Gene therapy for visual loss, Opportunities and concerns. Prog. Retin. Eye Res. *68*, 31–53.
16. DiCarlo, J.E., Mahajan, V.B., and Tsang, S.H. (2018). Gene therapy and genome surgery in the retina. J. Clin. Invest. *128*, 2177–2188.
17. Dinculescu, A., Estreicher, J., Zenteno, J.C., Aleman, T.S., Schwartz, S.B., Huang, W.C., Roman, A.J., Sumaroka, A., Li, Q., Deng, W.T., et al. (2012). Gene therapy for retinitis pigmentosa caused by MFRP mutations, human phenotype and preliminary proof of concept. Hum. Gene Ther. *23*, 367–376.
18. Dinculescu, A., Min, S.H., Deng, W.T., Li, Q., and Hauswirth, W.W. (2014). Gene therapy in the rd6 mouse model of retinal degeneration. Adv. Exp. Med. Biol. *801*, 711–718.

19. Velez, G., Tsang, S.H., Tsai, Y.T., Hsu, C.W., Gore, A., Abdelhakim, A.H., Mahajan, M., Silverman, R.H., Sparrow, J.R., Bassuk, A.G., and Mahajan, V.B. (2017). Gene therapy restores Mfrp and corrects axial eye length. Sci. Rep. *7*, 16151.

20. Wei, J., Ran, G., Wang, X., Jiang, N., Liang, J., Lin, X., Ling, C., and Zhao, B. (2019). Gene manipulation in liver ductal organoids by optimized recombinant adeno-associated virus vectors. J. Biol. Chem. *294*, 14096–14104.

21. Ran, G., Chen, X., Xie, Y., Zheng, Q., Xie, J., Yu, C., Pittman, N., Qi, S., Yu, F.X., Agbandje-McKenna, M., et al. (2020). Site-directed mutagenesis improves the transduction efficiency of capsid library-derived recombinant AAV vectors. Mol. Ther. Methods Clin. Dev. *17*, 545–555.

22. Zheng, Q., Wang, T., Zhu, X., Tian, X., Zhong, C., Chang, G., Ran, G., Xie, Y., Zhao, B., Zhu, L., and Ling, C. (2021). Low endotoxin E. coli strain-derived plasmids reduce rAAV vector-mediated immune responses both in vitro and in vivo. Mol. Ther. Methods Clin. Dev. *22*, 293–303.

23. Katada, Y., Kobayashi, K., Tsubota, K., and Kurihara, T. (2019). Evaluation of AAV-DJ vector for retinal gene therapy. PeerJ *7*, e6317.

24. Li, Q., Miller, R., Han, P.Y., Pang, J., Dinculescu, A., Chiodo, V., and Hauswirth, W.W. (2008). Intraocular route of AAV2 vector administration defines humoral immune response and therapeutic potential. Mol. Vis. *14*, 1760–1769.

25. Sullivan, J.A., Stanek, L.M., Lukason, M.J., Bu, J., Osmond, S.R., Barry, E.A., O'Riordan, C.R., Shihabuddin, L.S., Cheng, S.H., and Scaria, A. (2018). Rationally designed AAV2 and AAVrh8R capsids provide improved transduction in the retina and brain. Gene Ther. *25*, 205–219.

26. Petrs-Silva, H., Dinculescu, A., Li, Q., Min, S.H., Chiodo, V., Pang, J.J., Zhong, L., Zolotukhin, S., Srivastava, A., Lewin, A.S., and Hauswirth, W.W. (2009). High-efficiency transduction of the mouse retina by tyrosine-mutant AAV serotype vectors. Mol. Ther. *17*, 463–471.

27. Wang, N., Zhou, P., Chen, Y., Qu, H., Lu, K., and Xia, J. (2020). MicroRNA-149, A review of its role in digestive system cancers. Pathol. Res. Pract. *216*, 153266.

28. Cao, Y., Wang, Z., Yan, Y., Ji, L., He, J., Xuan, B., Shen, C., Ma, Y., Jiang, S., Ma, D., et al. (2021). Enterotoxigenic bacteroidesfragilis promotes intestinal inflammation and malignancy by inhibiting exosome-packaged miR-149-3p. Gastroenterology *161*, 1552–1566.e12.

29. Jiang, R., Zhang, H., Zhou, J., Wang, J., Xu, Y., Zhang, H., Gu, Y., Fu, F., Shen, Y., Zhang, G., et al. (2021). Inhibition of long non-coding RNA XIST upregulates microRNA-149-3p to repress ovarian cancer cell progression. Cell Death Dis. *12*, 145.

30. Zhou, L., and Xu, X.L. (2021). Long non-coding RNA ARAP1-AS1 facilitates the progression of cervical cancer by regulating miR-149-3p and POU2F2. Pathobiology *88*, 301–312.

31. Kay, C.N., Ryals, R.C., Aslanidi, G.V., Min, S.H., Ruan, Q., Sun, J., Dyka, F.M., Kasuga, D., Ayala, A.E., Van Vliet, K., et al. (2013). Targeting photoreceptors via intravitreal delivery using novel, capsid-mutated AAV vectors. PLoS One *8*, e62097.

32. Mowat, F.M., Gornik, K.R., Dinculescu, A., Boye, S.L., Hauswirth, W.W., Petersen-Jones, S.M., and Bartoe, J.T. (2014). Tyrosine capsid-mutant AAV vectors for gene delivery to the canine retina from a subretinal or intravitreal approach. Gene Ther. *21*, 96–105.

33. Gonzalez-Cordero, A., Goh, D., Kruczek, K., Naeem, A., Fernando, M., Kleine Holthaus, S.M., Takaaki, M., Blackford, S.J.I., Kloc, M., Agundez, L., et al. (2018). Assessment of AAV vector tropisms for mouse and human pluripotent stem cell-derived RPE and photoreceptor cells. Hum. Gene Ther. *29*, 1124–1139.

34. McClements, M.E., Steward, H., Atkin, W., Goode, E.A., Gándara, C., Chichagova, V., and MacLaren, R.E. (2022). Tropism of AAV vectors in photoreceptor-like cells of human iPSC-derived retinal organoids. Transl. Vis. Sci. Technol. *11*, 3.

35. Wiley, L.A., Burnight, E.R., Kaalberg, E.E., Jiao, C., Riker, M.J., Halder, J.A., Luse, M.A., Han, I.C., Russell, S.R., Sohn, E.H., et al. (2018). Assessment of adeno-associated virus serotype tropism in human retinal explants. Hum. Gene Ther. *29*, 424–436.

36. Dalkara, D., Byrne, L.C., Klimczak, R.R., Visel, M., Yin, L., Merigan, W.H., Flannery, J.G., and Schaffer, D.V. (2013). In vivo-directed evolution of a new adeno-associated virus for therapeutic outer retinal gene delivery from the vitreous. Sci. Transl. Med. *5*, 189ra76.

37. Byrne, L.C., Day, T.P., Visel, M., Strazzeri, J.A., Fortuny, C., Dalkara, D., Merigan, W.H., Schaffer, D.V., and Flannery, J.G. (2020). In vivo-directed evolution of adeno-associated virus in the primate retina. JCI Insight *5*, e135112.

38. Qiao, C., Yuan, Z., Li, J., Tang, R., Li, J., and Xiao, X. (2012). Single tyrosine mutation in AAV8 and AAV9 capsids is insufficient to enhance gene delivery to skeletal muscle and heart. Hum. Gene Ther. Methods *23*, 29–37.

39. Rashid, K., Wolf, A., and Langmann, T.((2018). Microglia activation and immunomodulatory therapies for retinal degenerations. Front. Cell. Neurosci. *12*, 176.

40. Xiong, W., Wu, D.M., Xue, Y., Wang, S.K., Chung, M.J., Ji, X., Rana, P., Zhao, S.R., Mai, S., and Cepko, C.L. (2019). AAV cis-regulatory sequences are correlated with ocular toxicity. Proc. Natl. Acad. Sci. USA *116*, 5785–5794.

41. Russell, S., Bennett, J., Wellman, J.A., Chung, D.C., Yu, Z.F., Tillman, A., Wittes, J., Pappas, J., Elci, O., McCague, S., et al. (2017). Efficacy and safety of voretigene neparvovec (AAV2-hRPE65v2) in patients with RPE65-mediated inherited retinal dystrophy, a randomised, controlled, open-label, phase 3 trial. Lancet *390*, 849–860.

42. Almoallem, B., Arno, G., De Zaeytijd, J., Verdin, H., Balikova, I., Casteels, I., de Ravel, T., Hull, S., Suzani, M., Destrée, A., et al. (2020). The majority of autosomal recessive nanophthalmos and posterior microphthalmia can be attributed to biallelic sequence and structural variants in MFRP and PRSS56. Sci. Rep. *10*, 1289.

43. Ho, K.L., Yong, P.H., Wang, C.W., Kuppusamy, U.R., Ngo, C.T., Massawe, F., and Ng, Z.X. (2022). Peperomia pellucida (L.) Kunth and eye diseases, A review on phytochemistry, pharmacology and toxicology. J. Integr. Med. *20*, 292–304.

44. Ran, G., Feng, X.L., Xie, Y.L., Zheng, Q.Y., Guo, P.P., Yang, M., Feng, Y.L., Ling, C., Zhu, L.Q., and Zhong, C. (2021). The use of miR122 and its target sequence in adeno-associated virus-mediated trichosanthin gene therapy. J. Integr. Med. *19*, 515–525.

45. Tian, X., Wang, T., Zhang, S., Wang, Q., Hu, X., Ge, C., Xie, L., and Zhou, Q. (2018). PEDF reduces the severity of herpetic simplex keratitis in mice. Invest. Ophthalmol. Vis. Sci. *59*, 2923–2931.